Validation of Fourier Transform Infrared Microspectroscopy for the Evaluation of Enzymatic Cross-Linking of Bone Collagen

Aleksandra Mieczkowska, Guillaume Mabilleau

Calcified Tissue International
https://doi.org/10.1007/s00223-023-01105-z

ORIGINAL RESEARCH

Validation of Fourier Transform Infrared Microspectroscopy for the Evaluation of Enzymatic Cross-Linking of Bone Collagen

Aleksandra Mieczkowska[1] · **Guillaume Mabilleau**[1,2]

Received: 2 March 2023 / Accepted: 26 May 2023

Abstract

Enzymatic cross-linking of the bone collagen is important to resist to crack growth and to increased flexural strength. In the present study, we proposed a new method for assessment of enzymatic cross-link based on Fourier transform infrared (FTIR) microspectroscopy that takes into account secondary structure of type I collagen. Briefly, femurs were collected from sham or ovariectomized mice and subjected either to high-performance liquid chromatography—mass spectrometry or embedded in polymethylmethacrylate, cut and analyzed by FTIR microspectroscopy. FTIR acquisition was recorded before and after ultraviolet (UV) exposure or acid treatment. In addition, femurs from a second animal study were used to compare gene expression of *Plod2* and *Lox* enzymes and enzymatic cross-links determined by FTIR microspectroscopy. We evidenced here that intensities and areas of subbands located at ~1660, ~1680, and ~1690 cm^{-1} were positively and significantly associated with the concentration of pyridinoline (PYD), deoxypyridinoline, or immature dihydroxylysinonorleucine/hydroxylysinonorleucine cross-links. Seventy-two hours exposure to UV light significantly reduced by ~86% and ~89% the intensity and area of the ~1660 cm^{-1} subband. Similarly, 24 h of acid treatment significantly reduced by 78% and 76% the intensity and area of the ~1690 cm^{-1} subband. *Plod2* and *Lox* expression were also positively associated to the signal of the ~1660 and ~1690 cm^{-1} subbands. In conclusion, our study provided a new method for decomposing the amide I envelope of bone section that positively correlates with PYD and immature collagen cross-links. This method allows for investigation of tissue distribution of enzymatic cross-links in bone section.

Keywords FTIR · Enzymatic collagen cross-linking · Pyridinoline · Hydroxypyridinoline · Collagen maturity

Introduction

The extracellular matrix of bone tissue is a composite material, consisting of type I collagen fibers (organic matrix, ~ 35–45% by volume), poorly crystalline carbonated hydroxyapatite crystals (mineral phase, ~35–45% by volume), and water (~15–25% by volume) [1]. Although type I collagen is the most ubiquitous protein in connective tissues, its chemistry varies from one tissue to another due to post-translational modifications and cross-linking [2]. Collagen cross-linking adds stability to the organic matrix, preventing the micro-fibrils from sliding over each other, allowing the cortical bone to better resist to crack growth and to increase bending strength of long bones [3].

Enzymatic collagen cross-linking occurs in the extracellular space; however, the nature of the cross-links depends on previous intracellular post-translational modifications of the collagen molecule [4]. The first step of enzymatic cross-linking is represented by the intracellular hydroxylation of lysine (Lys) residue within the triple helix by lysyl hydroxylases 1 and 3 [5] and within telopeptides by lysyl hydroxylase 2 [6] leading to the formation of hydroxylysine residue (Hyl). In the extracellular space, Lys and Hyl residues can be converted to aldehydes, respectively, Lys^{ald} and Hyl^{ald}, by the action of lysyl oxidase. These aldehydes then initiate a series of condensation reactions with vicinal Lys^{ald}, Lys, Hyl, and histidine residues to form intra and intermolecular covalent cross-links [7]. In bone, the predominant enzymatic cross-links found are the divalent immature cross-links, dehydrodihydroxylysinonorleucine (deH-DHLNL),

✉ Guillaume Mabilleau
guillaume.mabilleau@univ-angers.fr

[1] Univ Angers, Nantes Université, ONIRIS, Inserm, UMR 1229, RMeS, REGOS, SFR ICAT, Université d'Angers, 49000 Angers, France

[2] CHU Angers, Departement de Pathologie Cellulaire et Tissulaire, UF de Pathologie osseuse, 49933 Angers, France

Published online: 06 June 2023

and dehydrohydroxylysinonorleucine (deH-HLNL) [8]. These immature cross-links are unstable, destroyed by acid treatment [9] and need to be reduced into their stable counterparts, dihydroxylysinonorleucine (DHLNL), and hydroxylysinonorleucine (HLNL), in order to be detected by LC–MS. Mature trivalent cross-links predominant in bone tissue are hydroxylysylpyridinoline (PYD), lysylpyridinoline (DPD) and pyrroles (Pyr).

The gold standard for the analysis of collagen cross-links is represented by liquid chromatography–mass spectrometry (LC–MS) [10]. However, LC–MS techniques are destructive and require bone samples to be powdered prior to analysis. With such setup, it is not possible to evaluate the distribution of collagen cross-links within a tissue despite recent evidences suggest that heterogeneity in collagen cross-link content is key for higher bone resistance to fracture [11]. Twenty-two years ago, Paschalis et al. proposed a spectroscopic method for the evaluation of collagen cross-links in bone tissue sections [12]. This methodology is based on Fourier transform infrared (FTIR) microspectroscopy analysis, in transmission mode, of the amide I and II spectral regions after second derivative and curve fitting. Paschalis et al. evidenced that two subbands located at ~1660 and ~1690 cm^{-1} corresponded to perturbation of carbonyl group vibrations due to PYD and deH-DHLNL [12]. More recently, Paschalis et al. also showed that not only the ~1660 cm^{-1} subbands was indicative of trivalent collagen cross-links but also the ~1680 cm^{-1} subband that seemed correlated to perturbation of carbonyl group vibrations due to the presence of DPD [13]. The 1660/1690 cm^{-1} ratio is now widely used worldwide as a marker of collagen maturity and represents an index of the maturation of divalent to trivalent cross-links. The 1660/1680 cm^{-1} is also more and more used as an indicator of enzymatic collagen cross-link ratio [14]. However, differences in FTIR spectral processing as compared with the original method reported by Paschalis et al., are often found and the validity of such maturity and cross-link ratios remains to be fully validated against gold-standard LC–MS method. Recently, the ~1678/1690 cm^{-1} ratio has also been proposed for investigation of advanced glycation end products in bone [15]. As such, better assignment of the subband located ~1680 cm^{-1} is required to appreciate the validity of newer outcome.

A second point of attention resides in the method used to identify subbands in Amide I spectral region. Indeed, by rigidly imposing the presence of subbands at 1633, 1660, and 1690 cm^{-1}, Farlay et al. were incapable of recording any significant decrease in enzymatic collagen cross-linking between controls and β-aminopropionitrile-treated animals [16]. However, when enzymatic collagen cross-links were measured by LC–MS, a significant reduction in PYD and DPD was observed between the two groups of animals. Interestingly, Belbachir et al. reported previously the presence of 9 subbands in the amide I band related to the secondary structure of type I collagen [17]. Moreover, 4 additional subbands could be present due to amino acid side chains [18]. In its seminal paper investigating enzymatic collagen cross-links by FTIR spectroscopy, Paschalis et al. described only 4 subbands in the amide I envelope of demineralized bovine bone [12]. More recently, Schmidt and coworkers reported their method of amide I decomposition that used seven gaussian subbands located between 1600 and 1710 cm^{-1} [15]. The spectral signatures of enzymatic collagen cross-linking overlap in the amide I band with spectral signature of the secondary structure of type I collagen and amino acid side chains. As such, it seems important to develop and validate a new method for decomposing the amide I signal that take into account the secondary structure of type I collagen and amino acid composition in order to accurately measure reducible divalent and non-reducible trivalent collagen cross-links. The accuracy of divalent and trivalent subbands needs also to be validated against gold standard LC–MS methodology for biological assignment.

In the present study, we reported a new second derivative spectroscopy-curve fitting algorithm based only on amide I spectral region and taking into account secondary structure of type I collagen and amino acid side chain for the determination of enzymatic collagen cross-links in bone tissue. Our method was compared with LC–MS determination of collagen cross-link content and the extent of gene expression of lysyl hydroxylase 2 and lysyl oxidase, two key enzymes involved in the initiation of enzymatic cross-linking.

Material and Methods

Animal Models

Evaluation of enzymatic collagen cross-linking was realized in bones of two animal studies. Supplementary Fig. 1 represents a schematic of the experimental protocol. In the first study, 20 BALB/c female mice (BALB/cJRj) were purchased from Janvier Labs (Janvier Labs, St Berthevin, France). Ten animals underwent Sham surgery at 12 weeks of age and the remaining ten animals underwent bilateral ovariectomy (OVX) under general anesthesia at the same age. Animals were sacrificed 4 weeks post-surgery. These animals were used for the correlation between collagen cross-links concentrations by High-performance liquid chromatography—mass spectrometry (HPLC–MS) and FTIR microspectroscopy. In the second study, bilateral OVX was performed in 8 BALB/c (BALB/cJRj) female mice at 12 weeks of age under general anesthesia. Eight sham operated BALB/c female mice with the same age were also used. These animals were used for the correlation between gene expression of *Plod2* and *Lox*, 2 key enzymes involved in enzymatic

collagen cross-linking [19, 20]. All animals were housed in social groups and maintained in a 12 h:12 h light:dark cycle and had free access to water and diet. At necropsy, uterus were collected and weighted to ensure optimum ovariectomy. Both femurs were also harvested and cleaned of soft tissues. Epiphyses were removed, and the bone marrow was flushed out with PBS (Study 1) or removed by centrifugation (Study 2) as proposed by Kelly et al. [21]. After bone marrow removal, left femurs were snap frozen in isotonic saline (Study 1) or RNAlater (Study 2) and store at − 80 °C until use. For both studies, right femurs were snap frozen in isotonic saline and stored at − 80 °C until use.

Processing of Bone Samples for the Evaluation of Collagen Cross-Links by FTIR Analysis

After overnight thawing at 4 °C, the right femur was fixed with 70% ethanol, dehydrated, cut transversally in half at the midpoint between third trochanter and distal condyle with a diamond saw, and embedded undecalcified in polymethylmethacrylate (pMMA). One-micrometer-thick cross section of proximal and distal part of the same femur was cut with an ultramicrotome (Leica EM UC7, Leica microsystems, Nanterre, France) and deposited on BaF2 windows. Spectral analysis was performed with a Bruker Hyperion 3000 infrared microscope coupled to a Vertex 70 spectrometer using a 64 × 64 focal plane array (FPA) detector. A field of view of 540 × 540 µm covering the posterior quadrant of the femur midshaft was analyzed. The spectrometer was filled with dessicant pellets to reduce the contribution of athmospheric water and CO_2. A 15× Cassegrain objective (NA 0.4) was used for all acquisition. The FPA detector was cooled down with liquid nitrogen for higher sensitivity. Mid-infrared spectra were recorded at a resolution of 4 cm^{-1} (spectral region 900–2000 cm^{-1}), with 32 accumulations in transmission mode. Background spectra were also recorded with the same specifications. Post-processing of spectra was done with a lab-made script written in Matlab and includes Mie scattering correction [22], pMMA subtraction, normalization of v1,v3 PO_4 peak to 1 and denoising using the Savitzky-Golay algorithm with a degree of 2 and a span length of 9. A quality control of each spectrum was performed by calculating the signal-to-noise ratio (SNR) over the spectral range 1850–2000 cm^{-1} free of biological signal. The SNR was computed as the ratio between the mean intensity on the spectral range 1850–2000 cm^{-1} over the standard deviation in the same spectral range. A SNR ≥ 10 was judged sufficient to continue the post-processing. Bone pixels were manually thresholded from bone marrow and resin using the v1,v3 PO_4 peak area. Non-bone pixels were excluded from further analysis. Spectra were further subjected to second derivative of the Amide I band (1590—1730 cm^{-1}) for identification of subband locations. With this method, the band constituting a given interval is revealed by the successive minima of the second derivative curve. For simplicity and automation in detection of subbands, we inverted the second derivative to identify successive maxima. Band assignment is presented in Table 1. Validation of subbands was based on secondary structure of type I collagen and signal occurring from perturbation of carbonyl group vibration at ~1660 and ~1690 cm^{-1}. Subband locations and widths at half maximum were then entered into a lab-written script that uses a Gaussian function for subband shape and allows the positioning with ± 3 cm^{-1} as compared with the location evidenced on the second derivative. Curve fitting was then processed to study separately the absorption bands of samples that may overlap in the amide I envelope. Spectral curve fitting quality was assessed by a root mean square error value set at 1% of the total spectral interval area. Intensities and areas of each subband were obtained. An example of the consequences of post-processing, second derivative, and curve fitting on FTIR spectra is presented in Supplementary Fig. 2. Interassay variability, measured on five consecutive acquisitions of hyperspectral cubes on the same field of view in five consecutive days, implying repetition of internal calibration of the FTIR spectrometer and detector cooling as well as post-processing of the hyperspectral cubes, was of 0.2%.

After first acquisition, bone sections of the proximal part of the femur were exposed to an ultraviolet (UV) light for 72 h at 4 °C using a mercury lamp and an Olympus U-MNU2 filter with an excitation at 360 nm. This treatment is known to degrade mature collagen cross-links. Similarly, bone sections from the distal part were exposed to 0.05 M

Table 1 Subpeak position and assignment

Position (cm^{-1})	Assignment
1602	Tyrosine side chain [18]
1609	*β*-turn [17]
1618	*β*-turn [17]
1628	Parallel *β*-sheet [17], Lysine side chain [18]
1639	Triple helix [17]
1647	Unordered structure [17]
1655	*α*-helix [17]
1662	Pyridinoline cross-link [12, 13]
1669	*β*-turn [17]
1674	Arginine side chain [18]
1682	Deoxypyridinoline cross-link [13], parallel *β*-sheet [17]
1689	DHLNL and HLNL cross-link [12]
1695	Anti-parallel *β*-sheet [17]
1708	Glutamic acid side chain [18]
1717	Aspartic acid side chain [18]
1723	

acetic acid at 4 °C for 24 h. This treatment is known to degrade labile immature collagen cross-links. Then proximal and distal sections were placed back to the FTIR microscope, and the same field of view as analyzed previously was subjected to second FTIR acquisition with the same settings as described above.

Processing of Bone Samples for the Evaluation of Collagen Cross-Links by HPLC–MS

Standards for pyridinoline (PYD, also known as hydroxylysylpyridinoline) and deoxypyridinoline (DPD, also known as lysylpyridinoline) were purchased from BOC Sciences, Inc. (catalog # 63800-01-1 and B2694-136861, respectively). Dihydroxylysinonorleucine (DHLNL) was purchased from Santa Cruz Biotechnology (Catalog # sc-207059B). Hydroxylysinonorleucine (HLNL) was purified from bovine tibia collected in a local slaughterhouse as described below for mouse bone. The left femur was frozen with liquid nitrogen and powdered using a multisample biopulverizer (Biospec, Cat. No. 59012MS), defatted in methanol/chloroform, extensively washed with deionized water and freeze-dried. The bone powder was then demineralized with 0.5 M EDTA pH 7.4 for 96 h at 4 °C, with renewal of the demineralization solution every day. The bone powder was then resuspended in phosphate buffer saline, and half of the resuspended powder was reacted with sodium borohydride (10 mg/ml in 1 mM NaOH with a ratio reagent/bone powder of 1:30 (w/w)) for 2 h at room temperature to preserve the immature collagen cross-Links [23]. Reduced and non-reduced samples were then washed, freeze-dried, and hydrolyzed in 6 M hydrochloric acid at 110 °C for 24 h as proposed in Gineyts et al. [24]. A portion of the acidic hydrolysate was used for hydroxyproline assay (HPLC assay Biorad). Values of collagen cross-links were then normalized to collagen content assuming 14% hydroxyproline by mass in collagen. The remainder of the acidic hydrolysate was cleaned on an SPE column (SPE Chromabond crosslinks, Macherey–Nagel). Briefly, 400 µl of sample hydrolysate was added to 2.4 ml of acetonitrile in a glass vial. This solution was then transferred to a SPE column previously equilibrated with a wash buffer made of 8 volume of acetonitrile, one volume of acid acetic, and one volume of deionized water. The SPE column was extensively washed four times with 2.5 ml of wash buffer and rinsed with 100 µl of deionized water. Collagen cross-links were eluted with 600 µl of 1% heptafluorobutyric acid (HFBA) in HPLC glass vials. Sixty microliters of this eluate were then analyzed by LC–MS using an Alliance 2795 module (Waters, Guyancourt, France) equipped with a Waters 2487 UV detector and coupled to a Bruker ESQUIRE 3000 + ESI ion trap mass spectrometer equipped with an electrospray source (Bruker, Wissembourg, France) assisted by the HyStar software (Bruker Daltonics). Briefly, collagen cross-links separation was performed using an Atlantis T3 reverse-phase column (3 µm, 4.6 × 100 mm) at 25 °C as proposed by Gineyts et al. [24]. The column flow rate was 1 ml/min. After the analytical column, the flow was split in half between fluorescence (0.6 ml/min) and MS (0.4 ml/min). Solvent A consisted in 0.12% of HBFA in 18 ohms pure water (as proposed and optimized by Gineyts et al.[24]) and solvent B was 50% acetonitrile. The column was equilibrated with 10% of solvent B prior to use, and chromatographic separation was achieved with a gradient elution from 10 to 20% solvent B in 40 min. PYD and DPD were monitored for fluorescence emission at 395 nm and excitation at 297 nm. The mass analyses were performed in positive ion mode. The target ions were $[M+H]^+$ at m/z 308 for DHLNL, m/z 292 for HLNL, m/z 429 for PYD and m/z 413 for DPD. The conditions were as follows: spray voltage of 4.5 kV, collision gas, He; collision energy amplitude, 1 V, nebulizer and drying gas, N2, 7L/min; pressure of nebulizer gas, 30 psi; dry temperature, 340 °C, m/z 100–1000.

Sixty microliters of the collagen cross-links eluate were also exposed for 72 h to UV light (excitation at 360 nm) prior to analysis by LC–MS as reported above.

Gene Expression Analysis

Gene expression analysis was performed after crushing the left femur in a liquid nitrogen-cooled biopulverizer. Nucleozol (Macherey–Nagel, Hoerdt, France) was added on top of the bone powder, and total RNA was purified with Nucleospin RNA set nucleozol column (Macherey–Nagel) according to the manufacturer recommendations. Total RNA was reversed transcribed using Maxima first-strand cDNA synthesis kit (Thermofisher Scientific, Illkirch-Graffenstaden, France). Real-time quantitative polymerase chain reaction (qPCR) was performed using TaqMan™ Fast advanced master mix and TaqMan Gene Expression Assays for *Lox* (Mm00495386_m1) and *Plod2* (Mm00478767_m1). The *B2m* endogenous control (Mm00437762_m1) was used for normalization using the $2^{-\Delta CT}$ method.

Statistical Analyses

Linear regression between concentration of PYD, DPD, DHLNL, and HLNL determined biochemically, *Plod2* or *Lox* expression and the intensity or relative area of the subpeaks located at ~1660, ~ 1680, and ~1690 cm^{-1} were performed using GraphPad Prism 8. Pearson correlation coefficient was computed to assess the direction and magnitude of covariation. Modification of intensity or relative area of subpeaks located at ~1660, ~1680, and ~1690 cm^{-1} before and after UV exposure or acidic treatment were compared using a paired t test. Differences were considered significant when $p < 0.05$.

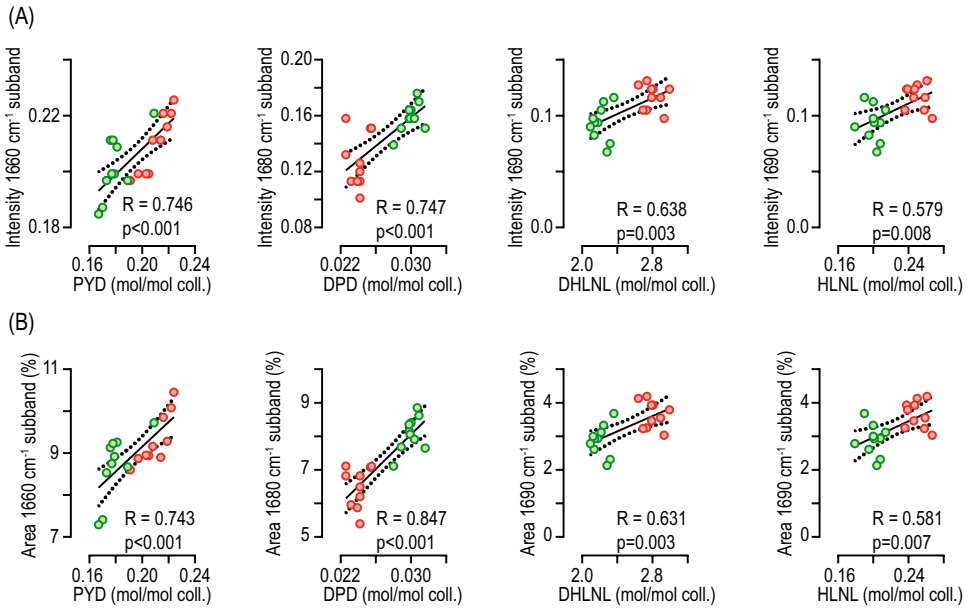

Fig. 1 Correlations between concentration of collagen cross-links determined by LC–MS and intensity or area of the ~1660, ~1680, and ~1690 cm^{-1} subbands. **A** Correlations between intensities of subbands and concentrations of pyridinoline (PYD), deoxypyridinoline (DPD), dihydroxylysinonorleucine (DHLNL), and hydroxylysinonorleucine (HLNL). **B** Correlations between area of subbands and concentrations of PYD, DPD, DHLNL, and HLNL. The Pearson correlation coefficient (R) was computed and a two-tailed *t* test was performed to assess the likelihood of random association between spectral and biochemical data, and considered significant at $p < 0.05$

Results

Positive Correlation Between Biochemical and Spectral Measurements of Enzymatic Collagen Crosslinks

As represented in Fig. 1 and as expected from previous work[13], pyridinoline (PYD) content, determined by LC–MS, was positively correlated with the intensity (R = 0.746, $p < 0.001$) and area (R = 0.743, $p < 0.001$) of the ~1660 cm^{-1} subband. Deoxypyridinoline (DPD) content was positively correlated with both the intensity (R = 0.747, $p < 0.001$) and area (R = 0.847, $p < 0.001$) of the ~1680 cm^{-1} subband. Furthermore, dihydroxylysinonorleucine (DHLNL) content and hydroxylysinonorleucine (HLNL) content, were also positively associated with both intensity (R = 0.638, $p = 0.003$ and R = 0.579, $p = 0.008$, respectively) and area (R = 0.631, $p = 0.003$ and R = 0.581, $p = 0.007$, respectively) of the ~1690 cm^{-1} subband.

Effects of UV Exposure on Mature Collagen Cross-Links

Due to small sample size, the strong correlation presented above may also be purely due to chance. We then decided to study whether UV exposure, known to destroy mature collagen cross-links, may modulate intensities and areas of ~1660 and ~1680 cm^{-1}. Indeed, PYD and DPD contents, measured by LC–MS, were reduced by 91% ($p < 0.001$) and 89% ($p < 0.001$), respectively, by this treatment (Fig. 2A). Changes in amide I envelope was also observed after UV exposure (Fig. 2B). Interestingly, intensity and area of the ~1660 cm^{-1} subband were drastically reduced by 86% ($p < 0.001$) and 89% ($p < 0.001$), respectively, suggesting that the biological entity contributing to this spectral signal was altered by UV exposure (Fig. 2C). On the other hand, intensity and area of the ~1680 cm^{-1} subband were augmented by 46% ($p < 0.001$) and 37% ($p < 0.001$), respectively, after UV exposure (Fig. 2C). These results were in opposition to the reduction of DPD content evidenced by LC–MS.

Effects of Acid Treatment on Divalent Collagen Cross-Links

As represented in Fig. 3A, the concentration of acid-labile divalent collagen cross-links was dramatically reduced by 99% ($p < 0.001$) for DHLNL (or its native non-reduced deH-DHLNL) and by 99% ($p < 0.001$) for HLNL (or its native non-reduced deH-HLNL), respectively. Here again, treatment of the bone section by 0.05 M acetic acid for 24 h resulted in changes in the amide I envelope (Fig. 3B). Intensity and area of the ~1690 cm^{-1} subband were significantly

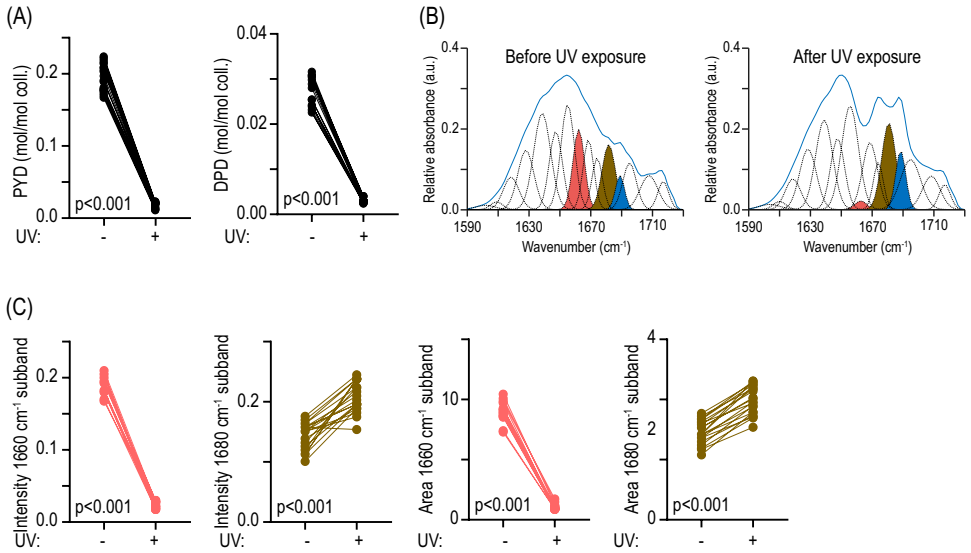

Fig. 2 Effects of UV exposure of mature collagen cross-links. Mature collagen cross-links are sensitive to UV exposure. **A** PYD and DPD concentrations were determined by LC–MS in two separate eluates that were exposed or not to UV light (360 nm) for 72 h. **B** The same bone section was imaged by FTIR before and after UV exposure for 72 h. Curve fitting of Amide I is presented and for clarity of subbands located at ~1660, ~1680 and ~1690 cm^{-1} were highlighted in pink, light brown, and blue, respectively. **C** Intensities and areas of ~1660 and ~1680 cm^{-1} subbands were computed on the same section prior to and after UV exposure for 72 h. Two-tailed paired *t* test were used to compute difference and were considered significant at $p < 0.05$

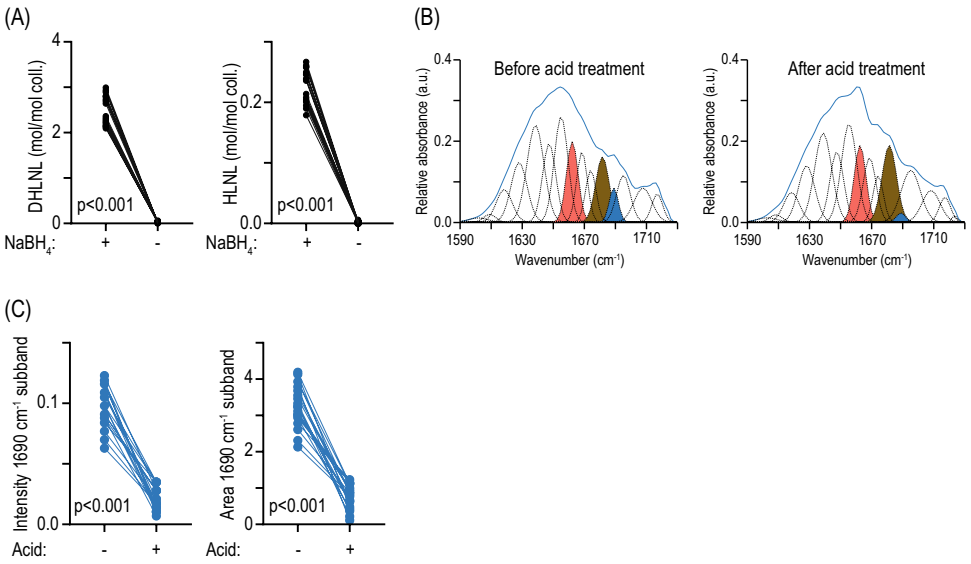

Fig. 3 Effects of acid treatment on immature collagen cross-links. Immature collagen cross-links are unstable and destroyed by acid. **A** For LC–MS analysis, half of the bone powder was not reduced by NaBH4 prior to matrix hydrolysis in 6 M HCl. The other half was reduced by $NaBH_4$ and protected immature collagen cross-links for destruction. **B** The same bone section was imaged by FTIR before and after treatment with acetic acid 0.05 M for 24 h. Curve fitting of Amide I is presented and for clarity of subbands located at ~1660, ~1680, and ~1690 cm^{-1} were highlighted in pink, light brown, and blue, respectively. **C** Intensities and areas of ~1690 cm^{-1} subband were computed. Two-tailed paired *t* test was used to compute difference and was considered significant at $p < 0.05$

decreased by 78% ($p < 0.001$) and 76% ($p < 0.001$), respectively.

Correlation Between Expression of *Plod2* and *Lox*, and Spectral Measurements of Enzymatic Collagen Cross-Links

We next assessed in bone of another study whether gene expression of *Plod2* and *Lox*, two enzymes involved in lysine hydroxylation and oxidation required for initiation of divalent collagen cross-links, were correlated to the area of ~1660, ~1680, and ~1690 cm^{-1} subbands. As presented in Fig. 4, *Plod2* expression was significantly and positively correlated with area of ~1690 cm^{-1} subband (R = 0.548, $p = 0.028$) and almost reach statistical for area of the ~1660 cm^{-1} (R = 0.487, p = 0.056). However, no correlation was found for area of the ~1680 cm^{-1} and *Plod2* expression (R = 0.242, $p = 0.367$). *Lox* expression was significantly and positively correlated with areas of ~1660 cm^{-1} (R = 0.502, $p = 0.048$) and ~1690 cm^{-1} (R = 0.681, $p = 0.004$) subbands. Here again, no correlation between *Lox* expression and area of the ~1680 cm^{-1} subband could be observed (R = 0.238, $p = 0.374$).

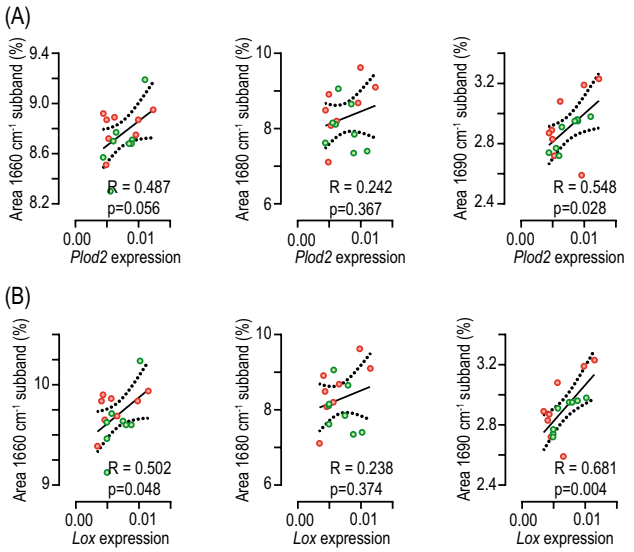

Fig. 4 Correlations between gene expression of key enzymes involved in collagen cross-linking and area of the ~1660 and ~1690 cm^{-1} subbands. **A** Correlations between level of *Plod2* expression and area of ~1660 and ~1690 cm^{-1} subbands. **B** Correlations between level of *Lox* expression and area of ~1660 cm^{-1} and ~1690 cm^{-1} subbands. The Pearson correlation coefficient (R) was computed and a two-tailed *t* test was performed to assess the likelihood of random association between spectral and biochemical data, and considered significant at $p < 0.05$. Green circle: data point from Sham animals; red circle: data point from OVX animals

Correlation Between 1660/1690 cm-1 Intensity and Area Ratios and PYD/(DHLNL + HLNL) Ratio

Finally, we assessed whether the 1660/1690 cm^{-1} intensity or area ratios were correlated with PYD/(DHLNL + HLNL) content measured by LC–MS (Fig. 5). We found positive correlation for both intensity and area ratios (R = 0.501, p = 0.025 and R = 0.571, $p = 0.009$, respectively) suggesting that these spectral ratios are indicative of trivalent over divalent collagen cross-links and, hence, collagen maturity.

Discussion

Collagen cross-links add stability to the organic matrix, preventing micro-fibrils from sliding over each other. Maturation of collagen cross-links is important to ensure resistance to crack growth but also bone strength [3, 25, 26]. In the present study, we proposed a new method of decomposition of the amide I band by FTIR spectroscopy that takes into account secondary structure of collagen. Although our method to assign subbands was based on second derivative, we employed more subbands than previously reported to account for secondary structure of type I collagen [12, 15]. Despite this modification of the original method developed by Paschalis and collaborators, we evidenced that intensities and areas of ~1660 and ~1690 cm^{-1} subbands were still positively correlated with the PYD and DHLNL/HLNL content of the collagen matrix, determined by LC–MS, but also the gene expression level of *Plod2* and *Lox*, two critical enzymes involved in collagen cross-link formation. Furthermore, changes in intensities and areas of the ~1660 cm^{-1}

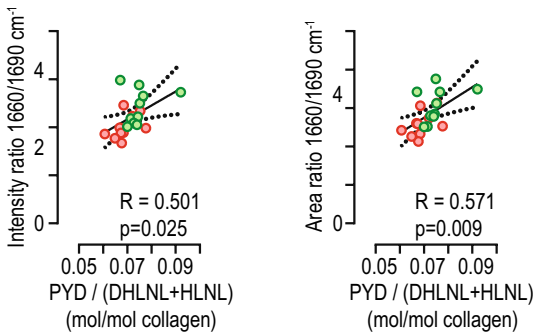

Fig. 5 Correlations between biochemical and spectral collagen maturity ratios. The biochemical ratio was computed as the concentration of the mature PYD over the sum of DHLNL and HLNL concentrations. The spectral ratio was computed as the intensity or area ratio of subbands located at ~1660 and ~1690 cm^{-1}. The Pearson correlation coefficient (R) was computed and a two-tailed *t* test was performed to assess the likelihood of random association between spectral and biochemical data, and considered significant at $p < 0.05$. Green circle: data point from Sham animals; red circle: data point from OVX animals

subband following UV exposure mimicked changes in PYD content determined by LC–MS. As expected, changes in intensities and areas of the ~1690 cm^{-1} subband after acid treatment also mirrored changes in DHLNL/HLNL content determined by LC–MS. These results are in agreement with previous studies where the ~1660 cm^{-1} was found correlated to PYD content and similar to changes reported after UV exposure [12, 13]. Interestingly, we evidenced a strong correlation between intensity and area of the ~1680 cm^{-1} subband and DPD content measured by LC–MS in agreement with previous observation of Paschalis et al. [13]. However, we did not observe a reduction in this subband intensity or area after UV exposure as one could expect. Furthermore, intensity and area of the ~1680 cm^{-1} subband were not correlated with the gene expression level of *Plod2* and *Lox* genes. The ~1680 cm^{-1} location has been shown to be a signature not only of advanced glycation end product but also of parallel β-sheet [15, 17]. The contribution of DPD to this underlying subband with our method remains to be fully validated as the correlation we observed between spectral and biochemical data might just be due to chance. This also imply that the ~1660/1680 cm^{-1} ratio is not a good marker of the extent of PYD and DPD in bone tissue.

However, the intensity and area ratios ~1660/1690 cm^{-1} correlated significantly with the PYD/(DHLNL + HLNL) biochemical ratio, suggesting that our method accurately decomposed the spectral signature of PYD and divalent collagen cross-links from secondary structure. This correlation is also in agreement with the seminal observations made by Paschalis et al. and suggest that when curve fitting is performed correctly, FTIR microspectroscopy is a valid method for assessing the extent of enzymatic collagen cross-linking. In opposition to LC–MS, FTIR microspectroscopy is non-destructive and allows an accurate assessment of enzymatic collagen cross-linking and when used in the imaging mode with a focal plane array detector, renders distribution of enzymatic collagen content in bone tissue sample. This is of interest as this methodology allows for investigation of cross-links heterogeneity in a tissue that could not be obtained by other technology.

Of note, we did not observe dramatic improvement of any correlation between intensity and area ratio with biochemical data. Although we cannot rule out an effect of specimen preparation on this matter, these observations also suggest that both intensity and area ratio could be used for determination of trivalent and divalent collagen cross-links in bone tissue section. This is not as surprising as in transmission mode, FTIR signal follows the Beer's law that uses intensity rather than area to link absorbance to concentration of an analyte. However, it is important to keep in mind that the ~1660 cm^{-1} and ~1690 cm^{-1} subbands are not direct measurement of PYD, DHLNL, and HLNL but rather are a reflect of the perturbation these cross-links exert on the carbonyl groups of collagen molecule. This is exemplified by lower intensity of the ~1690 cm^{-1} intensity as compared with the ~1660 cm^{-1} subband despite higher content of divalent cross-links than PYD measured by LC–MS.

The originality of our study also consists in a double validation against LC–MS gold standard but also gene expression of key enzyme involved in collagen cross-linking. This approach of correlating gene expression levels with spectral data has not yet been used for bone tissue, but was employed for breast tissue [27].

The relationship between bone toughness and enzymatic collagen cross-linking is up to now a controversial question. At the nanoscale, molecular stretching/unwinding competes with intermolecular sliding and breaking of weak and strong bonds between tropocollagen molecules. Previous investigations suggested that enzymatic collagen cross-links and collagen maturity are inversely correlated with plastic energy and, hence, bone toughness [28, 29]. Same correlation have also been observed with non-enzymatic collagen glycation [30]. However, inhibition of lysyl oxidase by β-aminopropionitrile that reduced PYD and DPD also demonstrated a strong and positive correlation between collagen maturity and bone toughness [3]. Furthermore, specific enhancement of enzymatic collagen cross-linking by gut hormone analogs also demonstrated enhancement of bone toughness [31].

In summary, we developed and validated in the present study a new method of amide I decomposition that takes into account secondary structure of collagen molecule and yet allows for accurate determination of PYD and enzymatic divalent cross-links of type I collagen in bone tissue section. This method confirms previous report that the ~1660 and ~1690 cm^{-1} subbands are indicative of PYD and divalent cross-link content. This method of spectral processing allows for investigation of tissue content and distribution of collagen cross-linking.

Supplementary Information The online version contains supplementary material available at https://doi.org/10.1007/s00223-023-01105-z.

Acknowledgements We are thankful to Prof Peter Gardner (University of Manchester) for supplying the Mie scattering correction routine for Matlab. We are also grateful to the institutional animal lab SCAHU, SFR ICAT 4208, Univ Angers, for their help with animal care.

Author Contributions AM: Investigation, Formal analysis and GM: Conceptualization, Investigation, Formal analysis, Writing—Review & Editing, Supervision, Funding acquisition, Data curation.

Funding This project was funded by an institutional grant from the University of Angers.

Data Availability The data that support the findings of this study are available from the corresponding author upon reasonable request.

Declarations

Competing interest Aleksandra Mieczkowska and Guillaume Mabilleau have no competing interests to declare that are relevant to the content of this article.

Ethical Approval All procedures were carried out in accordance with the European Union Directive 2010/63/EU for animal experiments and were approved by the regional ethical committee for animal use (authorization CEEA-PdL06-01740.01).

References

1. Granke M, Does MD, Nyman JS (2015) The role of water compartments in the material properties of cortical bone. Calcif Tissue Int 97:292–307
2. Yamauchi M, Sricholpech M (2012) Lysine post-translational modifications of collagen. Essays Biochem 52:113–133
3. McNerny EM, Gong B, Morris MD, Kohn DH (2015) Bone fracture toughness and strength correlate with collagen cross-link maturity in a dose-controlled lathyrism mouse model. J Bone Miner Res 30:455–464
4. Eyre DR, Paz MA, Gallop PM (1984) Cross-linking in collagen and elastin. Annu Rev Biochem 53:717–748
5. Uzawa K, Grzesik WJ, Nishiura T, Kuznetsov SA, Robey PG, Brenner DA, Yamauchi M (1999) Differential expression of human lysyl hydroxylase genes, lysine hydroxylation, and cross-linking of type I collagen during osteoblastic differentiation in vitro. J Bone Miner Res 14:1272–1280
6. Saito T, Terajima M, Taga Y, Hayashi F, Oshima S, Kasamatsu A, Okubo Y, Ito C, Toshimori K, Sunohara M, Tanzawa H, Uzawa K, Yamauchi M (2022) Decrease of lysyl hydroxylase 2 activity causes abnormal collagen molecular phenotypes, defective mineralization and compromised mechanical properties of bone. Bone 154:116242
7. Trackman PC (2016) Enzymatic and non-enzymatic functions of the lysyl oxidase family in bone. Matrix Biol 52–54:7–18
8. Yamauchi M, Katz EP, Otsubo K, Teraoka K, Mechanic GL (1989) Cross-linking and stereospecific structure of collagen in mineralized and nonmineralized skeletal tissues. Connect Tissue Res 21:159–167
9. Bailey AJ, Peach CM, Fowler LJ (1970) Chemistry of the collagen cross-links. Isolation and characterization of two intermediate intermolecular cross-links in collagen. Biochem J 117:819–831
10. Bielajew BJ, Hu JC, Athanasiou KA (2020) Collagen: quantification, biomechanics, and role of minor subtypes in cartilage. Nat Rev Mater 5:730–747
11. Wang ZX, Lloyd AA, Burket JC, Gourion-Arsiquaud S, Donnelly E (2016) Altered distributions of bone tissue mineral and collagen properties in women with fragility fractures. Bone 84:237–244
12. Paschalis EP, Verdelis K, Doty SB, Boskey AL, Mendelsohn R, Yamauchi M (2001) Spectroscopic characterization of collagen cross-links in bone. J Bone Miner Res 16:1821–1828
13. Paschalis EP, Gamsjaeger S, Tatakis DN, Hassler N, Robins SP, Klaushofer K (2015) Fourier transform Infrared spectroscopic characterization of mineralizing type I collagen enzymatic trivalent cross-links. Calcif Tissue Int 96:18–29
14. Wolfel EM, Schmidt FN, Vom Scheidt A, Siebels AK, Wulff B, Mushumba H, Ondruschka B, Puschel K, Scheijen J, Schalkwijk CG, Vettorazzi E, Jahn-Rickert K, Gludovatz B, Schaible E, Amling M, Rauner M, Hofbauer LC, Zimmermann EA, Busse B (2022) Dimorphic mechanisms of fragility in diabetes mellitus: the role of reduced collagen fibril deformation. J Bone Miner Res 37:2259–2276
15. Schmidt FN, Zimmermann EA, Campbell GM, Sroga GE, Puschel K, Amling M, Tang SY, Vashishth D, Busse B (2017) Assessment of collagen quality associated with non-enzymatic cross-links in human bone using Fourier-transform infrared imaging. Bone 97:243–251
16. Farlay D, Duclos ME, Gineyts E, Bertholon C, Viguet-Carrin S, Nallala J, Sockalingum GD, Bertrand D, Roger T, Hartmann DJ, Chapurlat R, Boivin G (2011) The ratio 1660/1690 cm(-1) measured by infrared microspectroscopy is not specific of enzymatic collagen cross-links in bone tissue. PLoS ONE 6:e28736
17. Belbachir K, Noreen R, Gouspillou G, Petibois C (2009) Collagen types analysis and differentiation by FTIR spectroscopy. Anal Bioanal Chem 395:829–837
18. Barth A (2007) Infrared spectroscopy of proteins. Biochim Biophys Acta 1767:1073–1101
19. Siegel RC, Fu JC (1976) Collagen cross-linking. Purification and substrate specificity of lysyl oxidase. J Biol Chem 251:5779–5785
20. van der Slot AJ, Zuurmond AM, Bardoel AF, Wijmenga C, Pruijs HE, Sillence DO, Brinckmann J, Abraham DJ, Black CM, Verzijl N, DeGroot J, Hanemaaijer R, TeKoppele JM, Huizinga TW, Bank RA (2003) Identification of PLOD2 as telopeptide lysyl hydroxylase, an important enzyme in fibrosis. J Biol Chem 278:40967–40972
21. Kelly NH, Schimenti JC, Patrick Ross F, van der Meulen MC (2014) A method for isolating high quality RNA from mouse cortical and cancellous bone. Bone 68:1–5
22. Bassan P, Sachdeva A, Kohler A, Hughes C, Henderson A, Boyle J, Shanks JH, Brown M, Clarke NW, Gardner P (2012) FTIR microscopy of biological cells and tissue: data analysis using resonant Mie scattering (RMieS) EMSC algorithm. Analyst 137:1370–1377
23. Bailey AJ (1968) Intermediate labile intermolecular crosslinks in collagen fibres. Biochim Biophys Acta 160:447–453
24. Gineyts E, Borel O, Chapurlat R, Garnero P (2010) Quantification of immature and mature collagen crosslinks by liquid chromatography-electrospray ionization mass spectrometry in connective tissues. J Chromatogr B Analyt Technol Biomed Life Sci 878:1449–1454
25. Gourion-Arsiquaud S, Faibish D, Myers E, Spevak L, Compston J, Hodsman A, Shane E, Recker RR, Boskey ER, Boskey AL (2009) Use of FTIR spectroscopic imaging to identify parameters associated with fragility fracture. J Bone Miner Res 24:1565–1571
26. Paschalis EP, Tatakis DN, Robins S, Fratzl P, Manjubala I, Zoehrer R, Gamsjaeger S, Buchinger B, Roschger A, Phipps R, Boskey AL, Dall'Ara E, Varga P, Zysset P, Klaushofer K, Roschger P (2011) Lathyrism-induced alterations in collagen cross-links influence the mechanical properties of bone material without affecting the mineral. Bone 49:1232–1241
27. Smolina M, Goormaghtigh E (2018) Gene expression data and FTIR spectra provide a similar phenotypic description of breast cancer cell lines in 2D and 3D cultures. Analyst 143:2520–2530
28. Berteau JP, Gineyts E, Pithioux M, Baron C, Boivin G, Lasaygues P, Chabrand P, Follet H (2015) Ratio between mature and immature enzymatic cross-links correlates with post-yield cortical bone behavior: An insight into greenstick fractures of the child fibula. Bone 79:190–195
29. Depalle B, Duarte AG, Fiedler IAK, Pujo-Menjouet L, Buehler MJ, Berteau JP (2018) The different distribution of enzymatic collagen cross-links found in adult and children bone result in different mechanical behavior of collagen. Bone 110:107–114
30. Acevedo C, Bale H, Gludovatz B, Wat A, Tang SY, Wang M, Busse B, Zimmermann EA, Schaible E, Allen MR, Burr DB, Ritchie RO (2015) Alendronate treatment alters bone tissues at

multiple structural levels in healthy canine cortical bone. Bone 81:352–363
31. Gobron B, Couchot M, Irwin N, Legrand E, Bouvard B, Mabilleau G (2023) Development of a first-in-class unimolecular dual GIP/GLP-2 analogue, GL-0001, for the treatment of bone fragility. J Bone Miner Res 38:733–748